## **EyePreserve: Identity-Preserving Iris Synthesis**

Siamul Karim Khan, Patrick Tinsley, Mahsa Mitcheff, Patrick Flynn, Kevin W. Bowyer, Adam Czajka University of Notre Dame

{skhan22, ptinsley, mmitchef, flynn, kwb, aczajka}@nd.edu

## **Abstract**

Synthesis of same-identity biometric iris images, both for existing and non-existing identities while preserving the identity across a wide range of pupil sizes, is complex due to the intricate iris muscle constriction mechanism, requiring a precise model of iris non-linear texture deformations to be embedded into the synthesis pipeline. This paper presents the first method of fully data-driven, identitypreserving, pupil size-varying synthesis of iris images. This approach is capable of synthesizing images of irises with different pupil sizes representing non-existing identities, as well as non-linearly deforming the texture of iris images of existing subjects given the segmentation mask of the target iris image. Iris recognition experiments suggest that the proposed deformation model both preserves the identity when changing the pupil size, and offers better similarity between same-identity iris samples with significant differences in pupil size, compared to state-of-the-art linear and non-linear (bio-mechanical-based) iris deformation models. Two immediate applications of the proposed approach are: (a) synthesis of, or enhancement of the existing biometric datasets for iris recognition, mimicking those acquired with iris sensors, and (b) helping forensic human experts examine iris image pairs with significant differences in pupil dilation. Images considered in this work conform to selected ISO/IEC 29794-6 quality metrics to make them applicable in biometric systems. The source codes and model weights are offered with this paper.

## 1. Introduction

Synthesis of same-identity biometric samples requires algorithms that preserve identity-related features, in addition to the preservation of visual realism. Realistic-looking irises can be synthesized by either older (non deep learning-based) algorithms [1], or by more recent models such as Generative Adversarial Networks [2, 3]. However, identity preservation, which involves modeling non-linear deformations of the iris texture pattern caused by pupil size change, is not offered by the existing approaches. In this paper, we introduce an identity-preserving mechanism that synthesizes same-eye biometric (*i.e.*, compliant with ISO/IEC 19794-6) iris images with varying pupil size, for both non-existing identities and existing iris samples. Our model pre-

serves the identity across generated samples, and also offers better biometric performance than a linear deformation approach [4] when there is a large dilation difference between probe and gallery images.

The core novel element of our solution is an autoencoder-based model trained to mimic intricate deformations of the iris muscle fibers when pupil dilation changes. The model input is (a) an iris image to be deformed and (b) a target iris shape defined by a binary mask indicating new locations of iris pixels. The model deforms the iris pattern to match a new iris shape employing its own "understanding" (learned from the data) of the iris texture deformation phenomenon. Experiments demonstrate that this iris texture deformation model offers better compensation for pupil size variations compared to the linear model [4], dominant in current iris recognition deployments, and a state-of-the-art non-linear bio-mechanical model [5]. Figure 1 provides an overview of how our method works.

The primary advantage of employing deep learningbased models is the elimination of the need for prior assumptions about iris muscle biomechanics, allowing the model to learn these features directly from videos of irises with varying pupil size. In summary, the novel contributions of this work are as follows.

- (a) a non-linear iris texture deformation model, operating on biometric iris images, not only preserving the identity but also offering better iris recognition performance when applied to normalize the pupil size compared to the state-of-the-art linear deformation model,
- (b) by adding Generative Adversarial Networks trained to generate ISO-compliant iris images, together with (a) the paper offers a complete method of synthesizing identity-preserving, pupil-size-varying iris images.

The source codes (including the training routines) and model weights are offered with this paper to facilitate replicability and various applications of this work: https://github.com/CVRL/EyePreserve.

## 2. Related Work

### 2.1. Iris Texture Deformation

Methods have been suggested for linear and non-linear iris texture deformation, which align iris texture patterns ac-

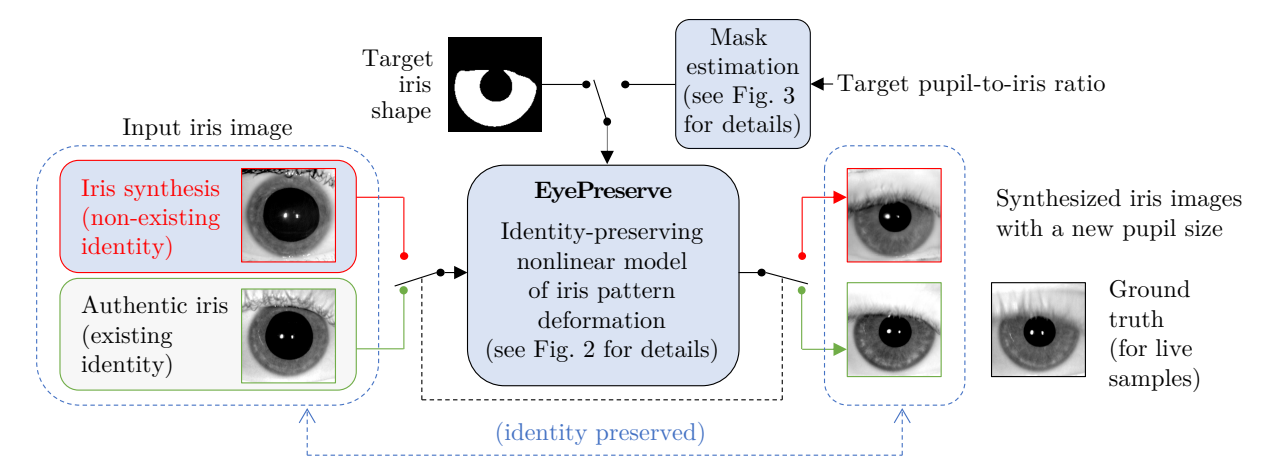


Figure 1. *EyePreserve* accepts (a) a ISO/IEC 29794-6-compliant iris image (either synthetically generated of a non-existing identity, or authentic of an existing subject) and (b) a new/target shape of the iris expressed either as a mask or a new pupil-to-iris ratio. By combining (a) and (b) the *EyePreserve* synthesizes a new ISO/IEC 29794-6-compliant iris image with the iris texture deformed to match a given new iris shape. The proposed model preserves the identity and correctly models non-linear deformations of the iris muscle. This paper also offers the model synthesizing irises of non-existing subjects, which creates a complete pipeline for identity-preserving iris image synthesis and deformation.

counting for elastic deformations of the iris muscles. In Daugman's "rubber sheet" model [4], the annular iris region is stretched to a fixed-sized rectangular block to account for pupil size changes. The limitation of this linear model is that significant pupil dilation can result in severe deviations from linear movements of the iris pattern. The Wyatt model [6] is a non-linear model based on Rohen's meshwork [7]<sup>1</sup> designed to minimize iris stretching as the pupil size changes. This is achieved by determining the optimal properties of the slopes between two arcs (fibers) and allowing points on a fiber to move only in the radial direction. The model introduced by Yuan and Shi [8] builds upon Wyatt's iris fiber structure by combining both linear and non-linear techniques and corrects scaling problems resulting from variations in distance. Reves et al. [5] introduced a biomechanical non-linear normalization where the iris is conceptualized as a thin cylindrical shell of orthotropic material, and the model calculates iris deformation in the radial direction using stress and strain vectors.

The above models were created to be part of the iris recognition pipeline, rather than to serve as identity-preserving elements of an iris synthesis pipeline. More recently, Khan *et al.* [9] proposed an autoencoder-based iris texture deformation model, developed and tested on iris images from a single source. Although this model was the first end-to-end, fully deep learning-based model of iris texture deformation, its identity preservation in a cross-dataset setting was not examined.

## 2.2. Synthetic Iris Image Generation

Researchers have recently investigated deep learning approaches for iris synthesis. Yadav *et al.* [2] applied a relativistic standard GAN (RaSGAN) to synthesize iris images used later to train iris presentation attack detection methods. This approach, however, did not offer control over the properties of synthesized irises, including the identity-related features. In [3], iWarpGAN was introduced to synthesize iris images not seen during training. It utilizes two distinct input images with different identities and styles. The generated image has a unique identity from the first input image and adopts the style of the second input image. Its limitation is that the number of new synthetic identities is the same as the number of real identities in the dataset.

In general, current generative models can change iris image styles, but none of them, to our knowledge, focuses on preserving the identity (synthetic or real) across different styles.

## 2.3. Identity Preservation in Biometric Data Synthesis

While preserving various object features, usually translating to visual/subjective realism, has been one of the main properties of image synthesis, the preservation of simultaneously biometric and human perception-assessed features has not yet been widely explored. Tzelepis *et al.* [10] introduced WarpedGANSpace, a method of face synthesis that aims to modify face styles by exploring radial basis function (RBF) paths in a GAN's latent space. The absence of matching scores for the different face styles does not allow us to fully assess the fidelity of identity preservation offered by this model.

<sup>&</sup>lt;sup>1</sup>The iris collagen structure is organized in a series of parallel fibers (arcs) connecting the pupil margin to the iris root (boundary) in clockwise and counterclockwise directions of 90 degrees.

Shoshan *et al.* [11], Liu *et al.* [12], and Li *et al.* [13] present controllable GAN models that are capable of generating face images of varying styles while preserving identity. Their models were developed in order to augment face recognition datasets to improve recognition accuracy and generalizability. FaceID-GAN [14], accomplishes the same task by adding a third model (a classifier component) to the GAN training process to encourage same-subject image synthesis. FaceFeat-GAN [15] preserves identity by introducing an intermediate feature generation and curation step before rendering the final image. Other works [16, 17] do not focus on synthesizing biometric data per se, but rather on re-styling authentic in-the-wild faces to fully frontal, neutral expression images. IPGAN [18] tries to preserve facial identity while creating caricature faces. Later, Li et al. [13] use a similar concept to maintain the identity and pose of a face in an input image while translating it to an image showing the face with different appearances and styles.

While identity preservation has been studied in face generation, iris image generation is more challenging as the identity information is embedded into higher frequency features.

#### 3. Datasets

The existing ISO/IEC 19794-6-compliant iris datasets usually lack samples acquired under intentional ambient light changes to control pupil dilation. Thus, we acquired samples from four distinct sources, as outlined in the following subsections, to enhance the model's ability to learn nonlinear deformations, and to provide comprehensive subject-disjoint evaluations of the proposed model.

### 3.1. Training Datasets

#### 3.1.1 Data Sources

Warsaw BioBase Pupil Dynamics (WBPD) [19] is composed of 159 high-resolution (768 × 576 px) iris videos from 42 individuals' eyes under varying lighting conditions (117,717 iris images in total). Each subject's eyes were captured at 25 FPS for 30 seconds: the first 15 seconds in darkness, next 5 seconds in elevated light intensity (pupil constriction period), and remaining 10 seconds in decreased light intensity (pupil dilation period). CSOSIPAD, is a subset of the "Combined Dataset" introduced by Boyd *et al.* in [20] that was used in conjunction with the WBPD dataset to inject more diversity into the training set for the models. Whereas WBPD had 84 different irises (42 subjects × 2 eyes), CSOSIPAD added 1,627 distinct irises (each iris is considered as a different identity).

#### 3.1.2 Training Data Curation

**WBPD-specific curation:** Iris images in which the iris texture was not visible were excluded from training. Furthermore, in order to avoid identity leakage (as described in e.g. [21]) and redundancy of very similar images seen during training, images in seconds 0-14 of each video were also excluded. After these two exclusions, 55,947 images remained. These images were centrally-cropped to a resolution of  $256 \times 256$ , with 16-pixel padding on each edge. **CSOSIPAD-specific curation:** Samples collected by the LG2200 sensor, which showed interlace artifacts, were removed. The remaining 50,167 CSOSIPAD images were centrally-cropped around the iris in the same manner as the WBPD data, and used for subsequent training.

Curation common for WBPD and CSOSIPAD: Our model training requires iris segmentation masks, which were generated with Vance *et al.*'s models [22]. Then we paired small- and large-pupil images so that we have appropriate inputs and targets to train the deformation model. To achieve this, we found the pupil and iris radii for all images in the WBPD and CSOSIPAD sets, and take all images with pupil-to-iris ratio between 0.2 and 0.7 (following suggestions from [5, 23]), divided into 5 bins of width 0.1, *i.e.*, the first bin contains images with pupil-to-iris ratios between 0.2 and 0.3, and so on. We pair images in each bin with images from all other bins.

#### 3.2. Test Datasets

The first test subset is an eye-disjoint subset of **WBPD** representing data from three subjects, whose data was not used during training and validation.

The second test set, the **Hollingsworth Split (HWS)** dataset [23] contains images of irises with pupil dilation variations for the same identities and was used to demonstrate that pupil dilation can degrade iris biometric performance. This dataset is technically an eye-disjoint subset of CSOSIPAD.

The third test set, the **Quality-Face/Iris Research Ensemble (Q-FIRE)** dataset [24], contains near-infrared (NIR) videos of individuals at different distances and illumination levels. We extract iris images from these videos using simple template-matching techniques and use the resulting dataset for evaluation. The source code for extracting still samples used in this work from the Q-FIRE videos are provided along with this paper to guarantee reproducibility.

Finally, the **CASIA-Iris-Lamp** (CIL) dataset [25], which is available as part of the CASIA-IrisV4 collection, consists of iris images taken using a handheld OKI iris sensor at different illumination levels.

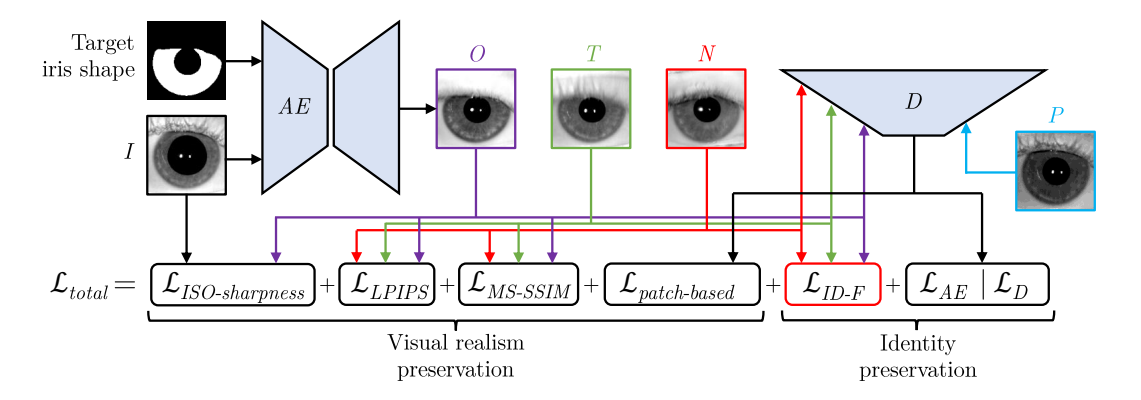


Figure 2. Illustration of the training mechanism with all loss function components explained in Sections 4.1.1 – 4.1.3. Symbols: I – input image, O – output image, T – target sample, N – negative (impostor) sample, P – positive (genuine) sample, D – discriminator, AE – autoencoder

## 3.3. Subject-Disjoint Train/Validation/Test Splits

The train, validation and test subsets are **eye-disjoint**. These eye-disjoint splits are imperative to ensure that the model is learning generic, biology-based iris muscle movements rather than dynamics specific to the eyes of subjects represented in the training dataset. To facilitate reproducibility of this work, all split definitions are offered as metadata along with this paper.

### 4. Iris Texture Deformation Model

## 4.1. Model Overview

To carry out identity-preserving iris texture deformation and get realistic variations of an eye image with different pupil sizes, we train an autoencoder that takes as input an undeformed iris image and a target iris shape defined by a binary mask to produce a deformed iris image. Fig. 2 provides an overview of how this autoencoder is trained. Subsections below discuss the proposed training strategy and model specifics, grouped into four categories: identity preservation, image/iris realism preservation, formulation of the triplet-based loss function combining all required components, and model architecture.

## 4.1.1 Identity Preservation

We utilize two loss components penalizing the model for not preserving the identity in a synthesized sample. The first, **filter-based identity preservation** loss component  $\mathcal{L}_{ID-\mathcal{F}}$  is defined as:

$$\mathcal{L}_{ID-\mathcal{F}}(I_1, I_2) = \| \mathcal{F}_{iris} \circledast N_D(I_1) - \mathcal{F}_{iris} \circledast N_D(I_2) \|$$
 (1)

where  $I_1$  and  $I_2$  are iris images being compared,  $N_D$  denotes Daugman's iris image normalization [4],  $\mathcal{F}_{iris}$  denotes a set of iris feature extraction filters,  $\circledast$  denotes the convolution operation, and  $\|\cdot\|$  denotes the  $L_1$  norm. To

create a comprehensive filter set assessing the biometric similarity between images, this loss component utilizes filters used in two open-source approaches: Gabor wavelets from OSIRIS [26] and human perception-derived filters from [27].

The second identity-preservation loss component is based on **adversarial training**. In generative modeling problems with classes of objects, the most commonly used architectural modification to the discriminator is the use of an auxiliary classifier [28] that assesses how well the discriminator synthesizes class exemplars. Thus, a naive approach would be to treat each identity as a separate class and train an auxiliary classification model along with the discriminator. However, this assumes that the total number of identities available in the training dataset is the complete set of identities possible.

Instead, our approach utilizes an adversarial identity loss, which allows the discriminator to learn embeddings from random triplets representing the same pupil-to-iris ratio and treat the output of the autoencoder as a separate identity pushing its embedding away from the target (anchor) and impostor (negative) identities. On the other hand, the autoencoder learns to produce an image that has the same embedding (from the discriminator) as the target (anchor) image but is different from the impostor (negative) image. We can formally define this adversarial loss component as follows. First, let  $\mathcal{L}_{cos}$  be the cosine loss, scaled to the  $\langle 0,1 \rangle$  range:

$$\mathcal{L}_{cos}(V_1, V_2) = 0.5(1 - CosSim(V_1, V_2))$$
 (2)

where CosSim is the cosine similarity. Let I be the input (undeformed) image, T be the target image, O be the output (deformed) image, P be the positive image that has the same identity as I and pupil-to-iris ratio as T, and N be the negative image that has a different identity but the same pupil-to-iris ratio as T. Let AE denote the autoencoder and

D denote the discriminator such that D(x) represents the embedding for an image x. For the loss of the autoencoder  $\mathcal{L}_{AE}$ , we have:

$$\mathcal{L}_{AE} = \mathcal{L}_{cos}(D(O), D(T)) + \mathcal{L}_{cos}(D(O), D(P))$$

$$+ \max \left(\mathcal{L}_{cos}(D(O), D(I)) - margin_{IT}, 0\right)$$

$$+ \max \left(margin_{NT} - \mathcal{L}_{cos}(D(O), D(N)), 0\right)$$
(3

where

$$margin_{IT} = \mathcal{L}_{cos}(D(I), D(T))$$

and

$$margin_{NT} = \mathcal{L}_{cos}(D(N), D(T)).$$
 (4)

Thus, to train the autoencoder, we first minimize the distance of the output image to both the target and the positive images (first line in eq. (3)). Secondly, we also minimize the distance between the output image and the input image as they belong to the same identity, but only as much as the loss between input and target, since the input image has a different pupil size than the target (second line in eq. (3)). Finally, we maximize the loss between the output and negative images, but only as much as the loss between the target and negative images (last line in Eq. (3)).

For the loss of the discriminator  $\mathcal{L}_D$ , we have:

$$\mathcal{L}_{D} = \max \left( \mathcal{L}_{cos} (D(T), D(P)) - \mathcal{L}_{cos} (D(T), D(N)) + margin_{D}, 0 \right)$$

$$+ \max \left( margin_{NTP} - \mathcal{L}_{cos} (D(O), D(T)), 0 \right)$$

$$+ \max \left( margin_{NTP} - \mathcal{L}_{cos} (D(O), D(P)), 0 \right)$$

$$+ \max \left( margin_{NTP} - \mathcal{L}_{cos} (D(O), D(N)), 0 \right),$$
(5)

where  $margin_D$  is a hyperparameter that defines the minimum separation required between the anchor and the positive images, while also specifying the maximum separation that has to be retained between the anchor and the negative images, and  $margin_{NTP}$  is an estimate of the maximum possible loss between impostor pairs of images with same pupil size, and is defined as:

$$margin_{NTP} = max(margin_{NT}, margin_{NP})$$

where  $margin_{NP} = \mathcal{L}_{cos}(D(N), D(P))$ , and  $margin_{NT}$  is defined by (4).

Therefore, the first part of the loss  $\mathcal{L}_D$  is a classical triplet margin loss between the target, positive, and negative images. This allows the discriminator to learn to distinguish iris images of different identities. In addition, with the subsequent components of the loss  $\mathcal{L}_D$ , the discriminator learns

to distinguish the autoencoder-generated image as different from the target, positive and negative images. In summary, the autoencoder tries to minimize the distance between embeddings of its output image and the original (target) image, while the discriminator tries to maximize this distance while simultaneously learning to distinguish between different identities.

#### 4.1.2 Realism Preservation

**Perceptual Losses:** To induce visual realism in the output images, we utilize two popular perceptual losses: the Learned Perceptual Image Patch Similarity (LPIPS) loss [29]  $\mathcal{L}_{LPIPS}$ , and Multi-Scale Structural Similarity (MS-SSIM) based loss [30]  $\mathcal{L}_{MS-SSIM}$ .

Adversarial Patch Loss: In our discriminator, we utilize the PatchGAN architecture [31] that learns to distinguish each image patch as real or fake. This image patch-based loss enables the model to enhance higher spatial frequencies to improve human visual perception of the synthesized images.

**ISO Sharpness Loss:** ISO/IEC 29794-6 SHARPNESS metric utilizes a single filtering kernel engineered to capture frequencies in an iris image that are essential for iris recognition. Let ISO be the ISO SHARPNESS score, O be the output image, and In be the input image. Then the ISO-sharpness loss

$$\mathcal{L}_{sharp}(O, In) = \max \left( ISO(In) - ISO(O), \ 0 \right)$$
 (6)

This loss ensures that the output image has the same or higher ISO SHARPNESS score as the input image provided to the autoencoder.

## 4.1.3 Triplet Formulation

A direct comparison between the output and target images should encourage a model to focus more on features that are common across the images. Thus, especially for losses such as  $\mathcal{L}_1$  and  $\mathcal{L}_2$ , this method of direct image comparison fails to capture distinctive features or to encourage high-frequency crispness. Consequently, for all of our identity-preservation losses ( $\mathcal{L}_{ID-\mathcal{F}}$ ,  $\mathcal{L}_{AE}$ ,  $\mathcal{L}_D$ ) and realism-preservation losses ( $\mathcal{L}_{LPIPS}$ ,  $\mathcal{L}_{MS-SSIM}$ ,  $\mathcal{L}_{sharp}$ ) we employ a triplet-based formulation:

$$\mathcal{L} := \mathcal{L}(O, T) + \max\left(margin - \mathcal{L}(O, N), 0\right) \tag{7}$$

where

$$margin = \mathcal{L}(T, Im).$$
 (8)

and O is the output image, T is the target image, and N is the negative (impostor) image.

The margin in the usual triplet loss defines the minimum possible value by which the anchor-negative loss should be higher than the anchor-positive loss. However, the margin in our formulation directly defines a value for the minimum possible anchor-negative loss. That is, in our triplet formulation, we utilize the fact that our output image should be as different from the impostor image as the target image should be, and take the loss between the target and the impostor image as the margin. By moving the output image away from an impostor image based on how much the target image is different from the impostor, while simultaneously moving the output image closer to the target, we encourage the model to generate images with more distinctive features rather than generating a blurry image capturing the common features across images.

### 4.1.4 Autoencoder Architecture

For our autoencoder, we utilize an attention-based nested U-Net similar to [32, 33]. However, we changed the downsampling operation from maxpooling to bilinear downsampling to improve the image generation capabilities. Note that any autoencoder architecture that has adequate image generation capabilities can be substituted for the autoencoder architecture we have used. That was intentional to allow this approach to generalize across many autoencoder architectures. Its strength comes from the composition of appropriate loss components.

## **5.** Associated Components

#### 5.1. Synthesis of Irises of Non-existing Identities

To propose the entire framework for pupil-varying, identity-preserving iris image synthesis, which also includes image synthesis for non-existing identities, we trained unconditional and conditional (*i.e.* with and without class label) StyleGAN-based models for iris image generation.

For the **unconditional** case, a StyleGAN3-based [34] model was trained on the combination of WBPD and CSOSIPAD datasets. Once the training process was completed, a new synthetic iris image could be generated using only a random seed and the corresponding "truncation" parameter value. As explained by the original StyleGAN authors, the "truncation trick" allows for balancing image quality with sample diversity. In order to generate a diverse set of realistically-looking synthetic images, a truncation value of 0.5 was used. The resultant images could then be used as the starting input image for the ensuing *EyePreserve* pipeline.

For the **conditional** case, a StyleGAN2-ADA model [35] was trained on the WBPD data. This framework includes training data augmentation techniques, enabling the training of a model even with a limited amount of data. The images

were selected with a pupil-to-iris ratio ranging from 0.2 to 0.7, encompassing the smallest and largest ratios within the WBPD dataset. Next, samples were divided into seven bins, ensuring that all bins were populated by approximately the same number of samples, ranging from 7,400 to 7,900. After completion of the model training, a random latent space vector was used in conjunction with a class label (*i.e.* condition) to generate iris images with different pupil sizes corresponding to the supplied condition. While conditional GANs provide control over selected properties of the image, we found that the identity is not well-preserved when altering the class condition while keeping a constant latent vector, as demonstrated in our evaluations illustrated in Fig. 5

## 5.2. Target Mask Estimation

The identity preservation component of the proposed solution requires comparing images of synthetically-generated images of irises having different pupil sizes and different palpebral fissure (eyelid opening). In such a comparison, we can deform one of the images to match the pupil size of the other image using the segmentation mask of the latter using our model. If we simply want to constrict/dilate an iris image given a new pupil "size", we can detect approximate circles for the pupil and iris using existing models, e.g. the one proposed in our previous work [22], and generate a circular mask corresponding to a new pupil radius. However, this approach would lead to "hallucinated" iris textures if the input iris image is occluded by eyelids. Thus, for synthesizing new iris images with a dilated pupil, we cut a larger pupil circle from the original (input) mask. To synthesize a new iris image with a constricted pupil, we fill out the pupil circle in the original (input) mask and then cut out a smaller pupil circle from it. This still leaves residual regions in the mask (from the larger pupil that was filled out) if there is occlusion by the eyelids. So, we use a segmentation model that segments the region inside the eyelids to discard any part of the mask outside the eyelid boundary. Figure 3 illustrates this procedure.

## 6. Assessment of Identity Preservation

To evaluate the identity-preserving capabilities of our system for both real and synthetically-generated iris images, we carry out evaluations on different datasets and iris recognition methods. The test datasets are described in section 3.2. Since the identity-preservation loss components used to train our model utilize filtering kernels from HDBIF [27] and OSIRIS [26] matchers, we also perform an evaluation with Dynamic Graph Representation for Occlusion Handling in Biometrics (DGR) [36] matcher to include iris encoding not used during training.

To estimate the uncertainty of the obtained results, and to report interval error estimates, we randomly sample 10%

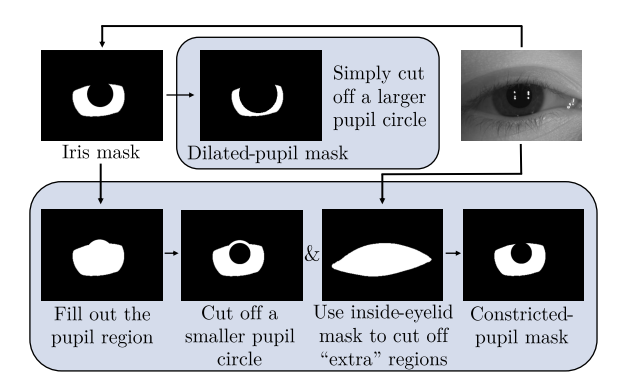


Figure 3. Illustration of the target iris image mask estimation. **Upper row:** Getting the target iris mask for dilated pupils is easy, and cut a larger pupil circle in the original mask. **Bottom row:** For the constricted-pupil iris mask, we need to fill out the pupil region and then cut a smaller pupil circle. However, when the pupil is partially occluded by eyelids, there are residual regions that we remove by using an "inside-eyelid" mask.

of our genuine and imposter pairs 100 times (with replacement) when calculating each Receiver Operating Characteristic (ROC) curves. We then report average Area Under ROC Curve (AUC) along with standard deviations of the AUC calculated over these 100 samples.

Section 6.1 demonstrates the identity preservation capabilities of the model when applied to slightly, moderately or significantly deformed iris texture. We show that the *EyePreserve* model does not degrade the matching performance when the correction for pupil size is small, and we also show that the *EyePreserve* model does improve significantly the performance when it is applied to correct large differences in pupil size. The following subsection 6.2 demonstrates experiments with conditional and uncoditional StyleGAN-based approaches, which – while being able to start from the GAN-inverted sample and synthesize iris images of varying pupil size – are not able to preserve identity adequately.

## 6.1. Deforming Images of Existing Irises

### **6.1.1** Scenario: Large Pupil Size Variations ( $\Delta > 0.3$ )

First, we analyze how *EyePreserve* performs when the difference in pupil size between the probe and gallery images is significant. We utilize the WBPD dataset which was specifically collected to study iris texture deformation under large pupil size variations, and thus contains a wide range of pupil sizes for the same eyes. A simple measure for the degree of pupil size change would be to calculate the difference in the pupil-to-iris ratio  $\Delta = \|p_1/i_1 - p_2/i_2\|$ , where p and i are pupil and iris radii, respectively [23].  $\Delta$  is large if one eye has a constricted pupil and the other has a dilated pupil, and small if pupil sizes are similar.

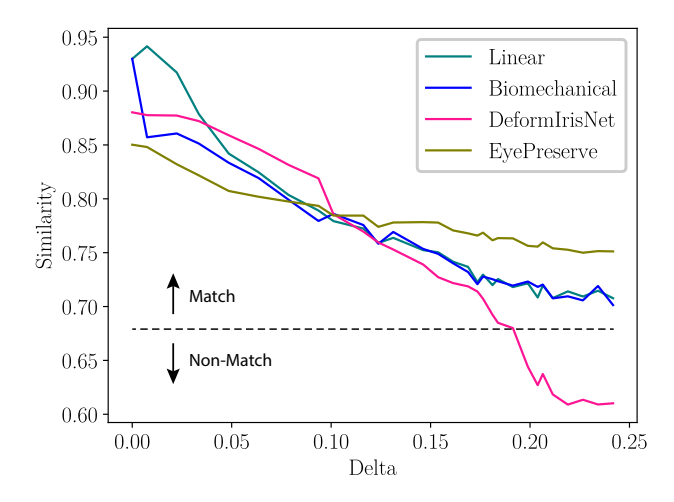
For each identity in the test set from WBPD, we compare the iris image with the largest pupil-to-iris ratio (highest dilation) with all the other images. We plot these comparison scores against the  $\Delta$  values for each iris deformation method. Figure 4 shows the results of these comparisons for a randomly picked identity in the test set. The curves for the rest of the identities are provided in the supplementary materials. From the graph, we can observe that our model is slightly worse than linear deformation. However, with a large-enough change in pupil size, our model performs better than a linear model. This occurs because initially the error caused by a linear deformation model is minute and the information loss due to passing the image through the Eye-Preserve model dominates the accuracy gain from the nonlinear deformation done by the EyePreserve. However, as we increase the amount of deformation, the actual iris texture deformation becomes significantly different from that estimated by a linear model, and the performance of EyePreserve offers significant gain over the linear model's performance.

These observations necessitated an evaluation of our model while considering the degree of change in pupil size for the other datasets as well. Due to the high fidelity of the WBPD data, low number of identities in the test set, and the data curation that was performed to remove almost-closed eves, the HDBIF method achieved almost perfect AUC on the test set with any method of iris deformation. Thus, the AUC values obtained for the HDBIF matcher does not show much on how the proposed model performs compared to the linear deformation model. The DGR method, however, showcases the changes in AUC as we compare in different ranges of  $\Delta$ . Table 1 summarizes results obtained by DGR on the WBPD dataset, which suggests that the proposed EyePreserve offers better modeling of iris texture deformation for larger differences between pupil size in the compared samples.

Table 1. Comparison of AUCs averaged over 100 samples with replacement consisting of 10% of the DGR comparison scores on the WBPD test set for different bins of  $\Delta$ . The standard deviation  $\epsilon \in [0.001, 0.002]$  in all variants.

Δ	Linear [4]	Diamashaniaal [5]	<b>EyePreserve:</b>	
		bioinechanicai [5]	Dilate	Dilate Constrict
[0, 0.1]	$0.996 \pm \epsilon$	$0.995 \pm \epsilon$	$0.996 \pm \epsilon$	$0.995 \pm \epsilon$
(0.1, 0.2]	$0.994 \pm \epsilon$	$0.995 \pm \epsilon$	$0.984 \pm \epsilon$	$0.992 \pm \epsilon$
(0.2, 0.3]	$0.991 \pm \epsilon$	$0.991 \pm \epsilon$	$0.992 \pm \epsilon$	$0.995 \pm \epsilon$
(0.3, 0.4]	$0.986 \pm \epsilon$	$0.985 \pm \epsilon$	$0.996 \pm \epsilon$	$0.995 \pm \epsilon$

It has been shown by Khan et al. [9] that the biomechanical model of iris texture deformation [5] performs about the same as the linear deformation [4]. The results obtained in this work and presented in Tab. 1 confirm this. Thus, in the rest of our evaluations, we compare our method with the more widely employed Daugman's linear deformation method instead of the biomechanical model.



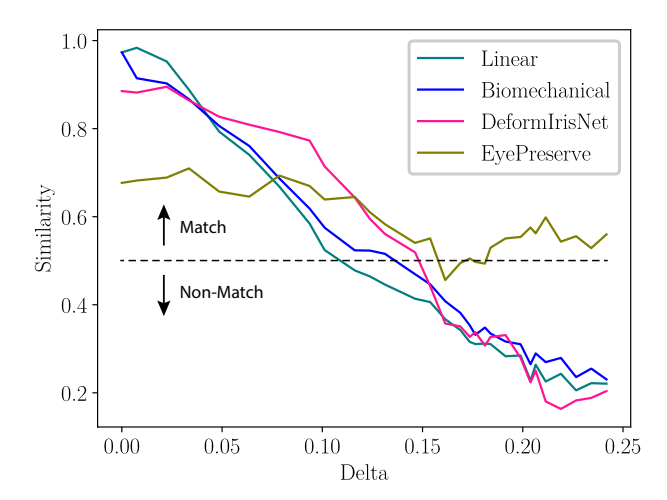


Figure 4. The similarity scores, offered by the HDBIF [27] (left) and DGR [36] (right) methods as a function of the pupil-to-iris ratio difference ( $\Delta$ ) between the probe and gallery samples. The dotted lines represent the similarity thresholds below which the image pair is considered a 'non-match' for a given matcher.

# **6.1.2** Scenario: Moderate Pupil Size Variations ( $\Delta > 0.2$ )

To further analyze how our model performs with pupil size variations, we utilize the HWS dataset (see Sec. 3.2). The pupil variation was achieved in this dataset by turning the ambient lighting off during the collection, which means that the iris muscles were not taken to their full range of motion. As such, the range of  $\Delta$  values is not as high as we find in the WBPD dataset, and hence this dataset replicates the real pupil size variations that may be observed in normal use of iris sensors more closely than the WBPD dataset.

We select samples from the HWS dataset with the largest possible difference  $\Delta$  in pupil size. To secure sufficient number of samples this translates to  $\Delta \geq 0.2$ , since the HWS dataset has very few pairs with  $\Delta > 0.3$ . Results presented in Tab. 2 suggest that our approach performs better than the classical Daugman's normalization routine when we are constricting the pupil. We believe this is happening because when we are dilating the pupil using our model, we are compressing the iris information into a smaller space, and then we are polar-normalizing using Daugman's model into a rectangular region to feed iris matchers with so preprocessed images. This could lead to a loss of features that are used by the iris matchers. The linear compensation in the way it is evaluated here does not suffer from this as we only carry out polar-normalization and, therefore, directly move to this rectangular region.

As seen in Tab. 2, the existing nonlinear deep learning-based iris deformation model, DeformIrisNet [9], does not generalize well to a new dataset.

Table 2. Comparison of AUCs averaged over 100 samples with replacements consisting of 10% of the comparison score for HDBIF and DGR on the subset of HWS-sourced pairs for which the **pupil dilation difference**  $\Delta \geq 0.2$ .

		HDBIF	DGR
Linear [4]		$0.995 \pm 0.002$	$0.973 \pm 0.008$
DeformIrisNet	[ <mark>9</mark> ]	$0.683 \pm 0.020$	$0.700 \pm 0.030$
EyePreserve:	Dilate	$0.986 \pm 0.005$	$0.966 \pm 0.013$
Lyci leseive.	Constrict	$0.996 \pm 0.002$	$0.983 \pm 0.007$

Table 3. Same as in Tab. 2 except that the AUCs were obtained on the subset of HWS-sourced pairs for which the **pupil dilation** difference  $\Delta \leq 0.1$ .

		HDBIF	DGR
Linear [4]		$0.996\pm0.001$	$0.991 \pm 0.002$
DeformIrisNet [9]		$0.629 \pm 0.012$	$0.691 \pm 0.015$
EyePreserve:	Dilate	$0.993 \pm 0.002$	$0.990 \pm 0.002$
Lyel leselve.	Constrict	$0.994 \pm 0.001$	$0.990 \pm 0.002$

## **6.1.3** Scenario: Small Pupil Size Variations ( $\Delta < 0.1$ )

The goal of this third experimental scenario is to check whether there is a significant impact on the iris recognition performance when there is little or no change in pupil size. For this purpose we consider three subsets that have never been seen during the EyePreserve training: (a) the subset of the HSW set with  $\Delta < 0.1$ , (b) Q-FIRE and (c) CIL. While Q-FIRE and CIL datasets contain images with varying pupil sizes, the possible number of pairs with  $\Delta > 0.2$  would not secure statistically significant evaluations. Hence we consider the Q-FIRE and CIL datasets entirely for this scenario

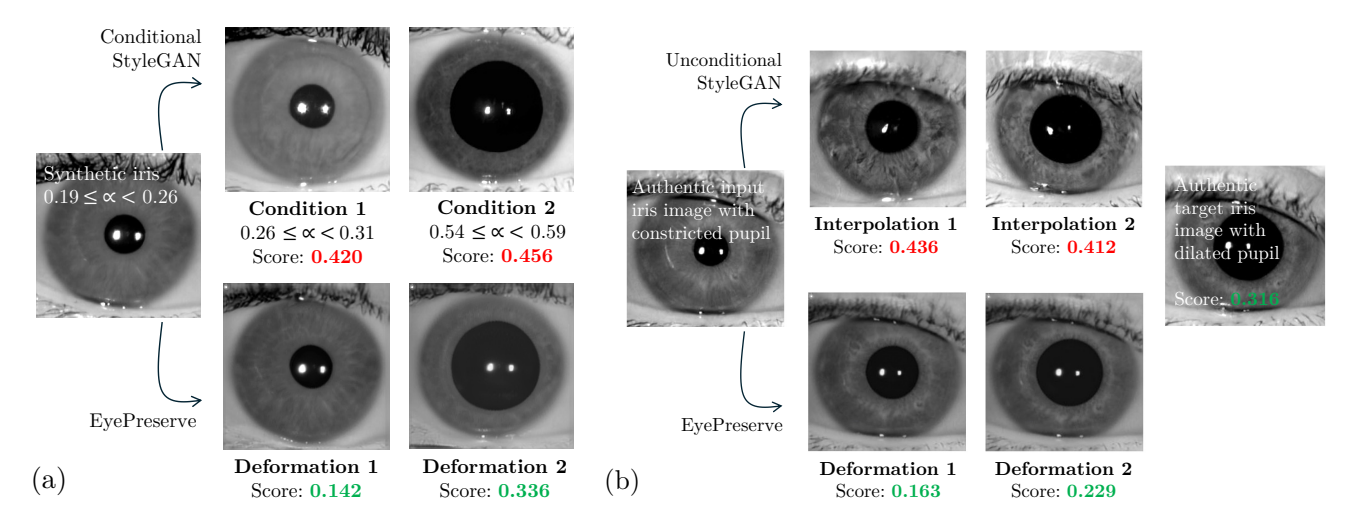


Figure 5. Illustration of how state-of-the-art StyleGAN models, conditional (a) and unconditional (b), solve the identity-preserving iris texture modeling. For a conditional model, the pupil size was encoded as a condition. For unconditional model, the varying pupil-size images were generated by traveling along the linearly interpolated path in StyleGAN's latent space between latent codes representing input and target images (after projecting images into the StyleGAN latent space). HDBIF scores in green (match) or red (non-match) are calculated between the left images and the synthesized samples. We observe that identity is not preserved between two iris images with different pupil size by both StyleGAN models, while it is preserved by the EyePreserve.

#### evaluation.

According to the results in Tables 3 and 4, the differences in iris recognition performance when a linear model and the EyePreserve model are applied are not statistically significant. A lower performance decrease observed for our model in case of the HDBIF matcher, and larged observed for the DGR matcher, could most likely be due to "hallucinated" textures when the target mask is larger (has more eyelid opening) than the input image. The DGR matcher is not using the masking mechanism proposed by Daugman, while the HDBIF matcher does, and hence discards any "dreamed-up" textures during comparisons appropriately.

The experiments and results in this subsection confirm that our goal of making the cost of propagating an iris image through EyePreserve – in a situation where there is no significant iris texture deformation that the model can "fix" – negligible was achieved.

Table 4. Comparison of AUCs averaged over 100 samples with replacements consisting of 10% of the comparison score for HDBIF and DGR on QFIRE and CIL datasets.

		Linear [4]	EyePreserve		
Dataset	Matcher	Linear [4]	Dilate	Constrict	
Q-FIRE	HDBIF	$0.995 \pm 0.001$	$0.996 \pm 0.001$	$0.996 \pm 0.001$	
	DGR	$0.976 \pm 0.004$	$0.955 \pm 0.004$	$0.958 \pm 0.004$	
CIL	HDBIF	$0.998 \pm 0.001$	$0.997 \pm 0.001$	$0.998 \pm 0.001$	
	DGR	$0.986 \pm 0.001$	$0.963 \pm 0.001$	$0.974 \pm 0.001$	

# **6.2. StyleGAN Models for Identity-Preserving Iris**Synthesis

Unconditional StyleGAN Although GANs have shown the ability to generate highly realistic iris images [2, 3, 21], the inner workings of these GANs' latent spaces are neither known nor predictable in the synthetic iris domain. For instance, linearly interpolating between small- and large-pupil images of the same iris in the StyleGAN's latent space W (as demonstrated in Fig. 5b) does not preserve identity. Although the endpoints of this interpolation process are images of the same iris, the intermediate interpolated images show iris textures that (a) do not match either endpoint, and (b) are recognizably fake. Contrarily, the proposed EyePreserve approach (bottom row in Fig. 5b), succeeds in maintaining identity for varying pupil dynamics, as can be seen in the green HDBIF scores.

Conditional StyleGAN Conditional GANs struggle to preserve identity, especially in the case of highly dilated irises. Also, they generate synthetic iris images similar to identities seen during training [21]. As depicted in Fig. 5a, this model failed to generate iris images with preserved identity using the same latent code but different conditions encoding the pupil size. As shown in the bottom row in Fig. 5b, the proposed EyePreserve model produced images with better matching scores for each pupil size.

### 6.3. Ablation Study

To better understand how the components of identity preservation loss and the components of perceptual loss interact

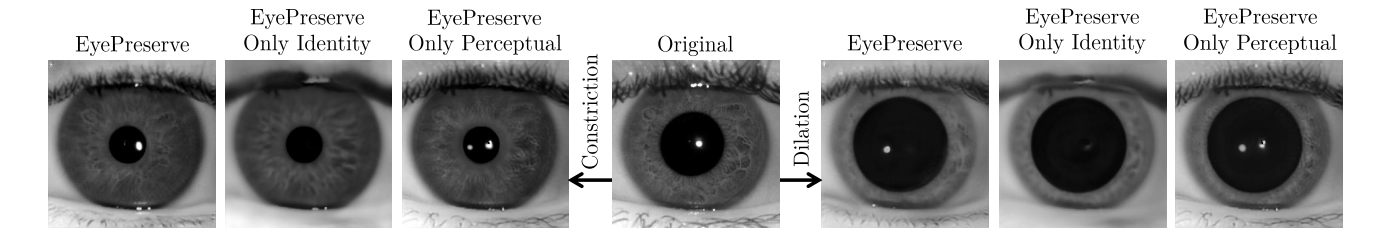


Figure 6. Visualization of synthesized iris images with different pupil-to-iris size ratios ( $\Delta$ ) for EyePreserve trained in three different scenarios: 1) with all of the losses, 2) with only the identity losses ( $\mathcal{L}_{ID-F}$ ,  $\mathcal{L}_{AE}$  and  $\mathcal{L}_{D}$ ), and 3) with only the perceptual losses ( $\mathcal{L}_{LPIPS}$ ,  $\mathcal{L}_{MS-SSIM}$ ,  $\mathcal{L}_{ISO-sharpness}$  and  $\mathcal{L}_{patch-based}$ ). Using only the identity losses causes the model to focus mostly on lower frequencies, resulting in blurrier generations that capture the larger-scale features in the iris texture. The opposite happens when only perceptual losses are used: the model focuses on higher frequencies, which leads to sharp images but can sometimes miss low-frequency identity-related features.

and affect the image generation process, we carry out an ablation study, in which we train our model with only the identity losses ( $\mathcal{L}_{ID-F}$ ,  $\mathcal{L}_{AE}$  and  $\mathcal{L}_{D}$ ) and only the perceptual losses ( $\mathcal{L}_{LPIPS}$ ,  $\mathcal{L}_{MS-SSIM}$ ,  $\mathcal{L}_{ISO-sharpness}$  and  $\mathcal{L}_{patch-based}$ ).

Table 5. Comparison of AUCs obtained for the EyePreserve model trained in three different scenarios: 1) with all of the losses, 2) with only the identity losses ( $\mathcal{L}_{ID-F}$ ,  $\mathcal{L}_{AE}$  and  $\mathcal{L}_{D}$ ), and 3) with only the perceptual losses ( $\mathcal{L}_{LPIPS}$ ,  $\mathcal{L}_{MS-SSIM}$ ,  $\mathcal{L}_{ISO-sharpness}$  and  $\mathcal{L}_{patch-based}$ ).

Dataset		Matcher	All Losses	Only Identity	Only Perceptual
HWS —	A < 0.1	HDBIF	0.9947	0.9950	0.9939
	$\Delta \le 0.1$	DGR	0.9804	0.9816	0.9746
	$\Delta \ge 0.2$	HDBIF	0.9953	0.9943	0.9909
		DGR	0.9686	0.9679	0.9195
Q-FIRE		HDBIF	0.9948	0.9944	0.9928
		DGR	0.9519	0.9552	0.9397
CIL		HDBIF	0.9947	0.9949	0.9924
		DGR	0.9716	0.9681	0.9660

Figure 6 illustrates how these different sets of losses affect the generated iris image, and Table 5 presents the results of iris recognition performance evaluation for each composition of the loss function. Using all losses and only identity losses results in about the same iris recognition performance; however, generated images are blurrier since iris recognition algorithms usually use lower spatial frequency content as biometric features. Also, we usually see a slight drop in performance when using only perceptual losses, since these losses focus on spatial image frequencies that are important from a human perception perspective, which may be different from those used by algorithms. We thus conclude that to obtain synthetic iris images that are usable in both automatic and human-based iris recognition, it is beneficial to use the entire set of loss components, as illustrated in Fig. 2.

## 7. Selected Applications Beyond Iris Matching

### 7.1. Rectification of Diseased-Deformed Irises

The EyePreserve model, although never trained for that purpose, can deform any shape of an iris to any other arbitrary shape, maximizing the preservation of identity-related features. That opens new, previously non-existent, applications of EyePreserve. One of them is "rectification" of iris images, which - due to diseases - have irregular pupil shapes. Fig. 7 visualizes a few sample inputs and outputs from our model for diseased iris images from Warsaw-BioBase-Disease-Iris v2.1 dataset [37] suffering from geometric deformations of the pupil. The target masks of the rectified images were estimated by (a) finding the outer iris boundary in the original (diseased iris) image, (b) cutting a pupil circle concentric with iris circle and ensuring a pupilto-iris ratio  $\alpha = 0.35$ , and (c) and then using the "insideeyelid" mask (cf. Fig. 3) to remove the remaining non-iris regions. Such rectification can be useful in human examination of iris images, especially for pairs of images representing irises before and after surgeries altering the iris structure or pupil shape.

To assess whether this rectification preserves identity, we performed an evaluation using HDBIF and DGR matchers, and compared the performance between obtained for the original (not rectified) images, and for those after rectification. We used a range of  $\alpha$  values between 0.2 and 0.7 with a step size of 0.05. As shown in Table 6, such rectification can be performed while preserving identity. Moreover this method achieved better performance for  $\alpha leg 0.4$  with the HDBIF-based matcher. We do not see similar improvements in the case of DGR, which creates a graph in which the iris features are graph nodes and the spatial relations between these features are edges. The irregular pupil shape gives rise to "strong" but fake features for the model, which uses them as nodes for its graph. When we rectify these irregularities, it loses these "strong" characteristics, leading to a slight and misleading loss in performance.

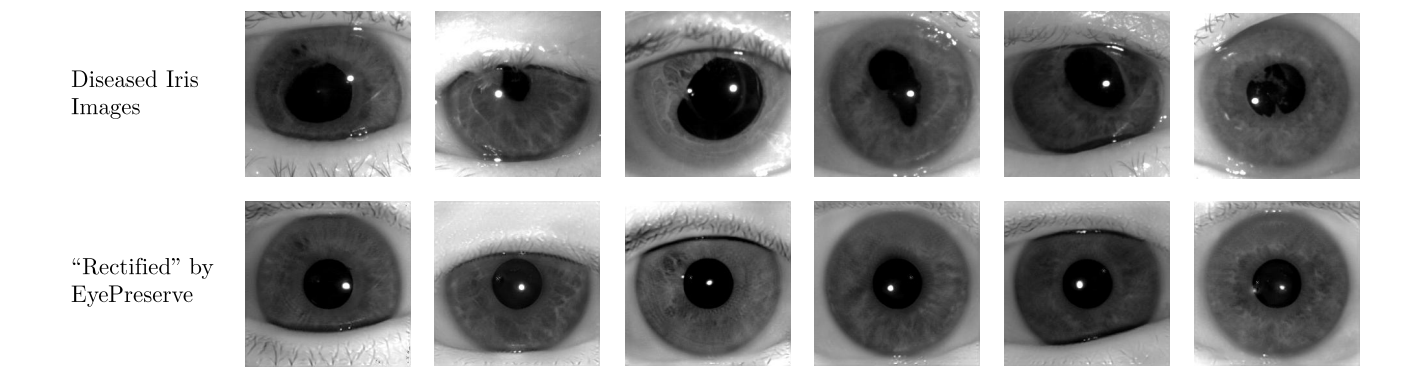


Figure 7. EyePreserve can rectify geometrical deformations of the iris texture caused by diseases, and make the pupil shape to be circular while preserving the subject's identity features. Samples of diseased eye images have been sourced from [37].

Table 6. Comparison of AUCs obtained before and after EyePreserve-based rectifications of geometric deformations caused by diseases (examples of such rectifications are shown in Fig. 7). The "geometry" subset of the dataset of images of diseased eyes [37] was used for this evaluation. For EyePreserve,  $\alpha$  is the pupil-to-iris ratio of the "rectified" iris image.

		HDBIF	DGR
Original Diseased ("Geometry" Set)		0.9894	0.9817
	$\alpha = 0.20$	0.9933	0.9534
	$\alpha = 0.25$	0.9949	0.9606
	$\alpha = 0.30$	0.9951	0.9657
	$\alpha = 0.35$	0.9948	0.9625
Diseased	$\alpha = 0.40$	0.9949	0.9584
("Geometry" Set)	$\alpha = 0.45$	0.9915	0.9547
Rectified	$\alpha = 0.50$	0.9883	0.9394
by EvePreserve	$\alpha = 0.55$	0.9873	0.9327
by Eyel Tesel ve	$\alpha = 0.60$	0.9821	0.9205
	$\alpha = 0.65$	0.9755	0.8799
	$\alpha = 0.70$	0.9175	0.8557

# 7.2. Morphing Iris Images into Irregular Pupil Shapes

The *EyePreserve* model's capabilities can be extended to deform the iris into arbitrary pupil shapes. Fig. 8 shows example results of modifying healthy iris images to mimic irregular pupil shapes that can be observed in diseased irises. Fig. 9 shows example deformations to arbitrary pupil shapes.

### 8. Conclusions

Complex deformations in the texture of the iris are difficult to model and require strong anatomical assumptions, which are often difficult to make. This paper proposes the first deep learning-based non-linear iris deformation model that generalizes well to unknown identities, along with a complete iris synthesis toolkit, which preserves identity when deforming the iris texture. The proposed model learns the visual appearance of the intricate iris muscle deformations without a need for often oversimplified anatomical assumptions and learns them quite effectively offering better performance of tested iris recognition methods compared to a state-of-the-art linear and non-linear (bio-mechanical-based) iris texture deformation models for significant differences in pupil dilation.

This work advances the iris recognition field in several ways: (a) offers better compensation of pupil dilation translating to better recognition performance compared to state-of-the-art models, especially in case of large differences in pupil size between the probe and galery samples, (b) by correct alignment of iris features it serves better the emerging field of forensic human experts-based iris examination, (c) it offers a complete pipeline of identity-preserving ISO/IEC-19794-6-compliant iris image synthesis, potentially enhancing recognition and presentation attack detection datasets.

## References

- [1] S. Makthal and A. Ross, "Synthesis of iris images using Markov Random Fields," in 2005 13th European Signal Processing Conference, 2005, pp. 1–4. 1
- [2] S. Yadav, C. Chen, and A. Ross, "Synthesizing Iris Images Using RaSGAN With Application in Presentation Attack Detection," in 2019 IEEE/CVF Conference on Computer Vision and Pattern Recognition Workshops (CVPRW), 2019, pp. 2422–2430. 1, 2, 9
- [3] S. Yadav and A. Ross, "iWarpGAN: Disentangling Identity and Style to Generate Synthetic Iris Images," in 2023 IEEE International Joint Conference on Biometrics (IJCB). IEEE, 2023, pp. 1–10. 1, 2, 9
- [4] J. G. Daugman, "High confidence visual recognition of persons by a test of statistical independence," *IEEE*



Modified by EyePreserve to mimic "irregular" pupil shapes observed in diseased irises















Figure 8. Opposite to what was demonstrated in Fig. 7, the EyePreserve model can modify healthy iris images to mimic irregular pupil shapes observed in diseased irises. The target image mask is the one estimated from an iris suffering from a diseases causing pupil shape distortions (in the example masks were estimated for samples shown in Fig. 7).

Original Image

Modified by EyePreserve to have arbitrary pupil shapes











Figure 9. Visualization of identity-preserving deformation of iris texture into arbitrary shapes. Videos depicting animations of these deformations are available in this paper's GitHub repository.

- *Trans. Pattern Anal. Mach. Intell.*, vol. 15, no. 11, pp. 1148–1161, 1993. 1, 2, 4, 7, 8, 9
- [5] I. Tomeo-Reyes, A. Ross, A. D. Clark, and V. Chandran, "A biomechanical approach to iris normalization," in *2015 International Conference on Biometrics (ICB)*. IEEE, 2015, pp. 9–16. 1, 2, 3, 7
- [6] H. J. Wyatt, "A 'minimum-wear-and-tear' meshwork for the iris," *Vision Research*, vol. 40, no. 16, pp. 2167–2176, 2000. 2
- [7] H. Rohen, "Der bau der regenbogenhaut beim menschen und einigen säugern," *Gegenbaur Morphology Journal*, vol. 91, pp. 140–181, 1951. 2
- [8] X. Yuan and P. Shi, "A non-linear normalization model for iris recognition," in *International Workshop on Biometric Person Authentication*. Springer, 2005, pp. 135–141.
- [9] S. K. Khan, P. Tinsley, and A. Czajka, "DeformIris-Net: An Identity-Preserving Model of Iris Texture Deformation," in *IEEE Winter Conference on Applications of Computer Vision (WACV)*, 2023, pp. 900–908. 2, 7, 8
- [10] C. Tzelepis, G. Tzimiropoulos, and I. Patras, "Warpedganspace: Finding non-linear rbf paths in gan latent space," in *Proceedings of the IEEE/CVF International Conference on Computer Vision*, 2021, pp. 6393–6402.
- [11] A. Shoshan, N. Bhonker, I. Kviatkovsky, and G. Medioni, "GAN-control: Explicitly controllable GANs," in *IEEE International Conference on Computer Vision (ICCV)*, 2021, pp. 14 083–14 093. 3
- [12] F. Liu, M. Kim, A. Jain, and X. Liu, "Controllable and guided face synthesis for unconstrained face recogni-

- tion," in *European Conference on Computer Vision*. Springer, 2022, pp. 701–719. **3**
- [13] T. Li, H. Zhao, J. Huang, and K. Li, "Cross-domain image translation with a novel style-guided diversity loss design," *Knowledge-Based Systems*, vol. 255, p. 109731, 2022. 3
- [14] Y. Shen, P. Luo, J. Yan, X. Wang, and X. Tang, "Faceid-gan: Learning a symmetry three-player gan for identity-preserving face synthesis," in *IEEE/CVF International Conference on Computer Vision and Pattern Recognition (CVPR)*, 2018, pp. 821–830. 3
- [15] Y. Shen, B. Zhou, P. Luo, and X. Tang, "Facefeat-GAN: a two-stage approach for identity-preserving face synthesis," *arXiv preprint arXiv:1812.01288*, 2018. 3
- [16] X. Zhu, Z. Lei, J. Yan, D. Yi, and S. Z. Li, "High-fidelity pose and expression normalization for face recognition in the wild," in *IEEE Trans. Pattern Anal. Mach. Intell.*, 2015, pp. 787–796. 3
- [17] X. Yin, X. Yu, K. Sohn, X. Liu, and M. Chandraker, "Towards large-pose face frontalization in the wild," in *IEEE International Conference on Computer Vision (ICCV)*, 2017, pp. 3990–3999. 3
- [18] L. Yan, W. Zheng, C. Gou, and F.-Y. Wang, "IP-GAN: Identity-Preservation Generative Adversarial Network for unsupervised photo-to-caricature translation," *Knowledge-Based Systems*, vol. 241, p. 108223, 2022. 3
- [19] J. Kinnison, M. Trokielewicz, C. Carballo, A. Czajka, and W. Scheirer, "Learning-free iris segmentation revisited: A first step toward fast volumetric operation

- over video samples," in 2019 International Conference on Biometrics (ICB). IEEE, 2019, pp. 1–8. 3
- [20] A. Boyd, J. Speth, L. Parzianello, K. W. Bowyer, and A. Czajka, "Comprehensive Study in Open-Set Iris Presentation Attack Detection," *IEEE Transactions on Information Forensics and Security*, vol. 18, pp. 3238–3250, 2023. 3
- [21] P. Tinsley, A. Czajka, and P. J. Flynn, "Haven't I Seen You Before? Assessing Identity Leakage in Synthetic Irises," in 2022 IEEE International Joint Conference on Biometrics (IJCB). IEEE, 2022, pp. 1–9. 3, 9
- [22] N. Vance, J. Speth, S. Khan, A. Czajka, K. W. Bowyer, D. Wright, and P. Flynn, "Deception Detection and Remote Physiological Monitoring: A Dataset and Baseline Experimental Results," *IEEE Transactions* on Biometrics, Behavior, and Identity Science, vol. 4, no. 4, pp. 522–532, 2022. 3, 6
- [23] K. Hollingsworth, K. W. Bowyer, and P. J. Flynn, "Pupil dilation degrades iris biometric performance," *Computer Vision and Image Understanding*, vol. 113, no. 1, pp. 150–157, 2009. 3, 7
- [24] P. A. Johnson, P. Lopez-Meyer, N. Sazonova, F. Hua, and S. Schuckers, "Quality in face and iris research ensemble (Q-FIRE)," in 2010 Fourth IEEE International Conference on Biometrics: Theory, Applications and Systems (BTAS), 2010, pp. 1–6. 3
- [25] Institute of Automation, Chinese Academy of Sciences, "CASIA-IrisV4," http://biometrics.idealtest.org/dbDetailForUser.do?id=4#/datasetDetail/4, 2020, dataset published by the Chinese Academy of Sciences' Institute of Automation. 3
- [26] N. Othman, B. Dorizzi, and S. Garcia-Salicetti, "OSIRIS: An open source iris recognition software," *Pattern Recognition Letters*, vol. 82, pp. 124–131, 2016. 4, 6
- [27] A. Czajka, D. Moreira, K. Bowyer, and P. Flynn, "Domain-specific human-inspired binarized statistical image features for iris recognition," in 2019 IEEE Winter Conference on Applications of Computer Vision (WACV). IEEE, 2019, pp. 959–967. 4, 6, 8
- [28] A. Odena, C. Olah, and J. Shlens, "Conditional image synthesis with auxiliary classifier gans," in *International Conference on Machine Learning*. PMLR, 2017, pp. 2642–2651. 4
- [29] R. Zhang, P. Isola, A. A. Efros, E. Shechtman, and O. Wang, "The unreasonable effectiveness of deep features as a perceptual metric," in *IEEE/CVF Inter*national Conference on Computer Vision and Pattern Recognition (CVPR), 2018. 5
- [30] Z. Wang, E. P. Simoncelli, and A. C. Bovik, "Multiscale structural similarity for image quality assessment," in *The Thrity-Seventh Asilomar Conference on*

- *Signals, Systems & Computers*, 2003, vol. 2. Ieee, 2003, pp. 1398–1402. 5
- [31] P. Isola, J.-Y. Zhu, T. Zhou, and A. A. Efros, "Image-to-image translation with conditional adversarial networks," in *IEEE/CVF International Conference on Computer Vision and Pattern Recognition (CVPR)*, 2017, pp. 1125–1134. 5
- [32] C. Li, Y. Tan, W. Chen, X. Luo, Y. He, Y. Gao, and F. Li, "ANU-Net: Attention-based nested U-Net to exploit full resolution features for medical image segmentation," *Computers & Graphics*, vol. 90, pp. 11–20, 2020. 6
- [33] C. Li, Y. Tan, W. Chen, X. Luo, Y. Gao, X. Jia, and Z. Wang, "Attention Unet++: A nested attention-aware u-net for liver CT image segmentation," in 2020 *IEEE International Conference on Image Processing* (ICIP). IEEE, 2020, pp. 345–349. 6
- [34] T. Karras, M. Aittala, S. Laine, E. Härkönen, J. Hellsten, J. Lehtinen, and T. Aila, "Alias-free generative adversarial networks," *Advances in Neural Information Processing Systems*, vol. 34, pp. 852–863, 2021.
- [35] T. Karras, M. Aittala, J. Hellsten, S. Laine, J. Lehtinen, and T. Aila, "Training generative adversarial networks with limited data," *Advances in neural information processing systems*, vol. 33, pp. 12104–12114, 2020. 6
- [36] M. Ren, Y. Wang, Z. Sun, and T. Tan, "Dynamic graph representation for occlusion handling in biometrics." in *AAAI*, 2020, pp. 11 940–11 947. 6, 8
- [37] M. Trokielewicz, A. Czajka, and P. Maciejewicz, "Assessment of iris recognition reliability for eyes affected by ocular pathologies," in 2015 IEEE 7th International Conference on Biometrics Theory, Applications and Systems (BTAS). IEEE, 2015, pp. 1–6. 10, 11

## Supplementary Material

This document presents the materials supplementing the Preserving Iris Synthesis results and illustrations provided in the main paper.

Figure 10 offers a full illustration of how the proposed model can morph iris images into arbitrary shapes (for the final results showed in the main paper in Fig. 9). The full videos showing these morphs are also available in the GitHub repository associated with this paper (https://github.com/CVRL/EyePreserve).

Additionally, we provide the histograms of genuine and impostor comparison scores for HDBIF and DGR matchers calculated with the WBPD test set samples (Figures 11 and 12), along with decidability score (d').

We found that the comparison score distributions for the proposed EyePreserve method have a higher separation than the score distributions obtained for a linear model in nearly all cases, as indicated by the higher d'. Certainly d' assumes that the comparison scores are normally distributed, so it only delivers an estimate of the separation between the score distributions.

Another interesting observation is a shift in all similarity scores to the right. We believe that this happens due to similar noise introduced by the neural network, which deforms all images before the comparisons (genuine or imposter) are being made. Hence higher similarity scores than those observed for unprocessed images.

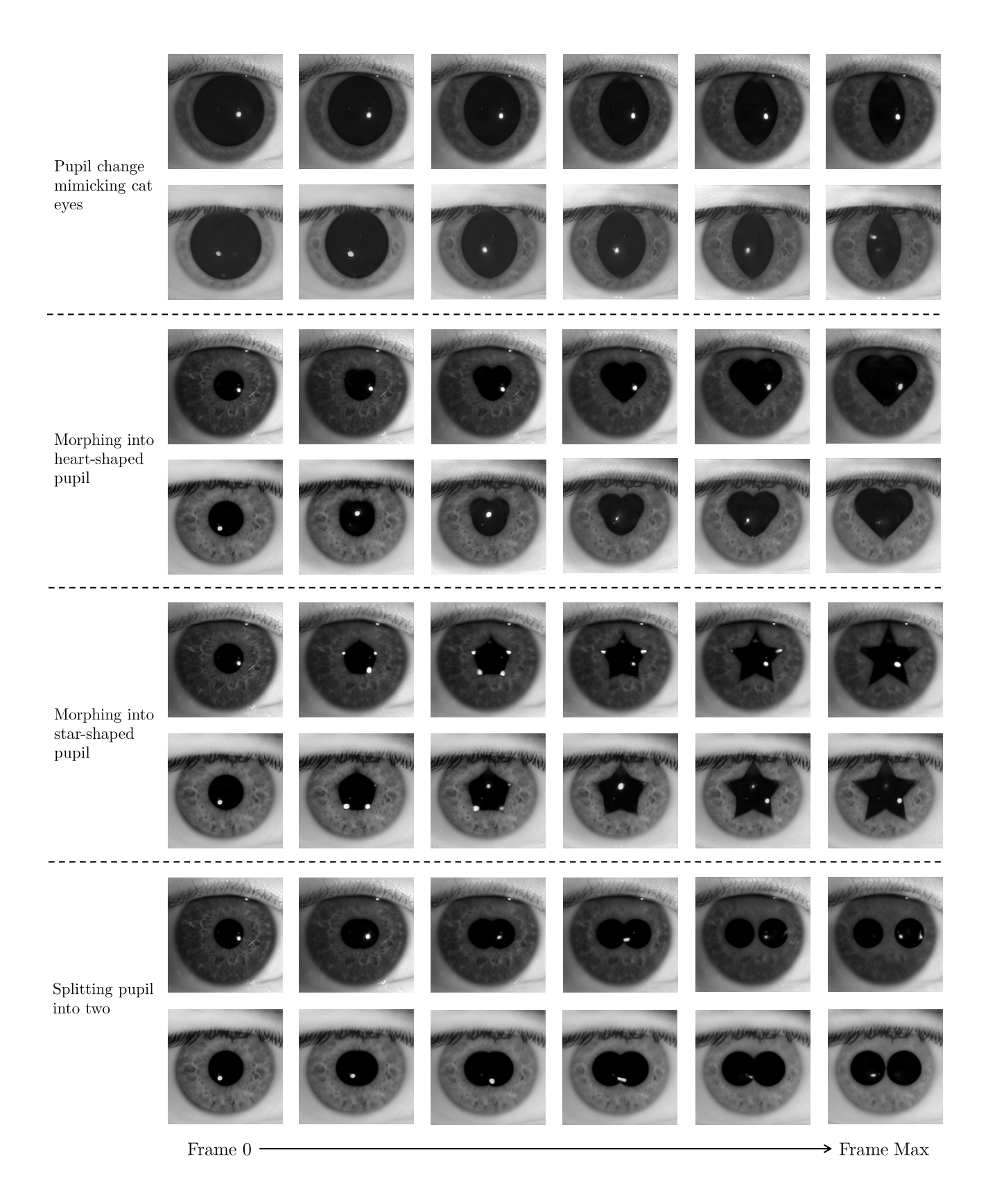


Figure 10. A more detailed look into morphing of the iris texture into an image with an arbitrary pupil shape. The animation videos for these morphs are available in our GitHub repo.

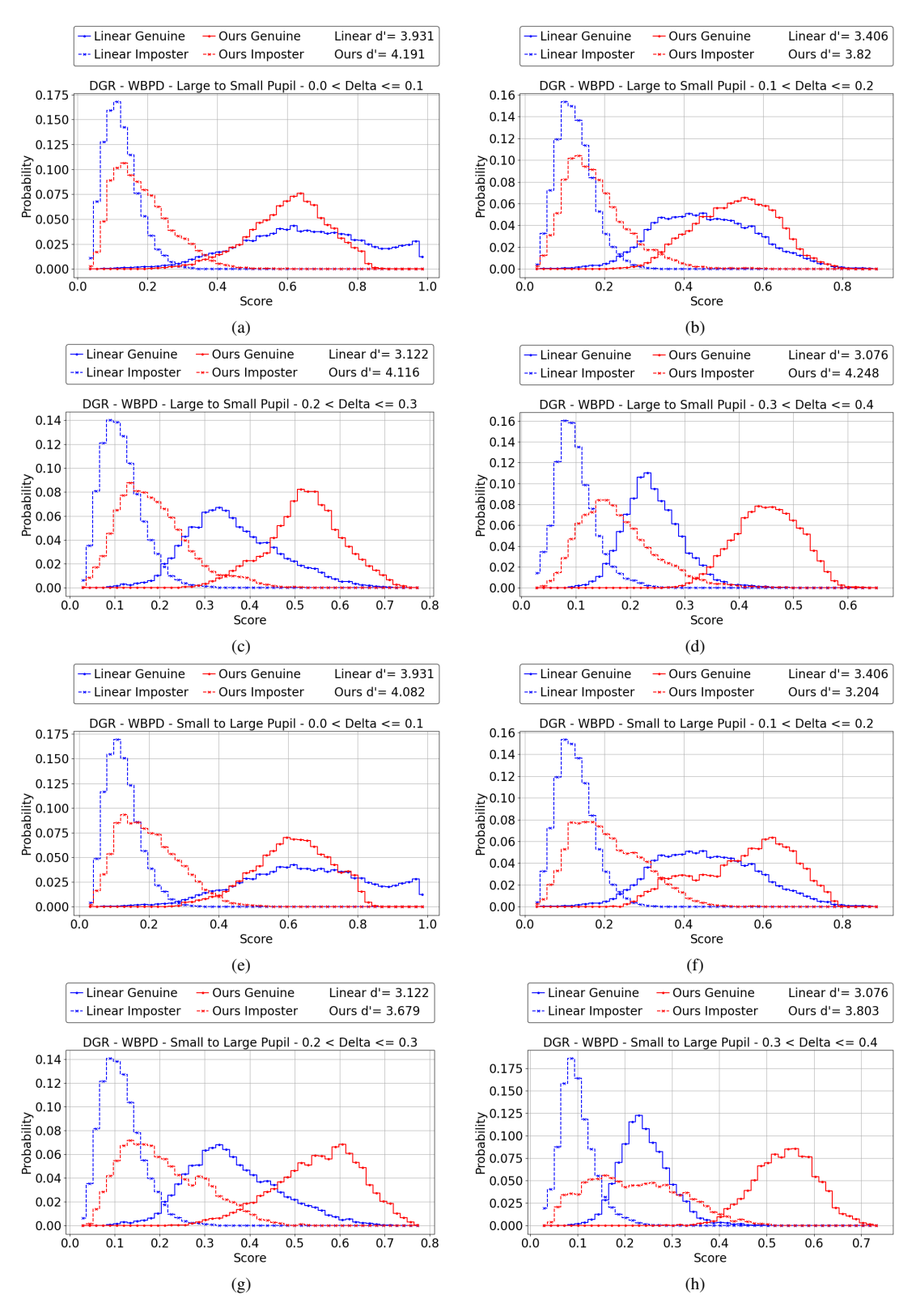


Figure 11. Histograms of comparison scores (the higher the score the more similar two images are) for the DGR matcher. Plots (a)-(d) show the scores for pupil **constriction difference**  $\Delta \in (0,0.1)$  (a),  $\Delta \in (0.1,0.2)$  (b),  $\Delta \in (0.2,0.3)$  (c) and  $\Delta \in (0.3,0.4)$  (d). Plots (e)-(h) show the scores for **pupil dilation difference**  $\Delta \in (0,0.1)$  (e),  $\Delta \in (0.1,0.2)$  (f),  $\Delta \in (0.2,0.3)$  (g) and  $\Delta \in (0.3,0.4)$  (h).

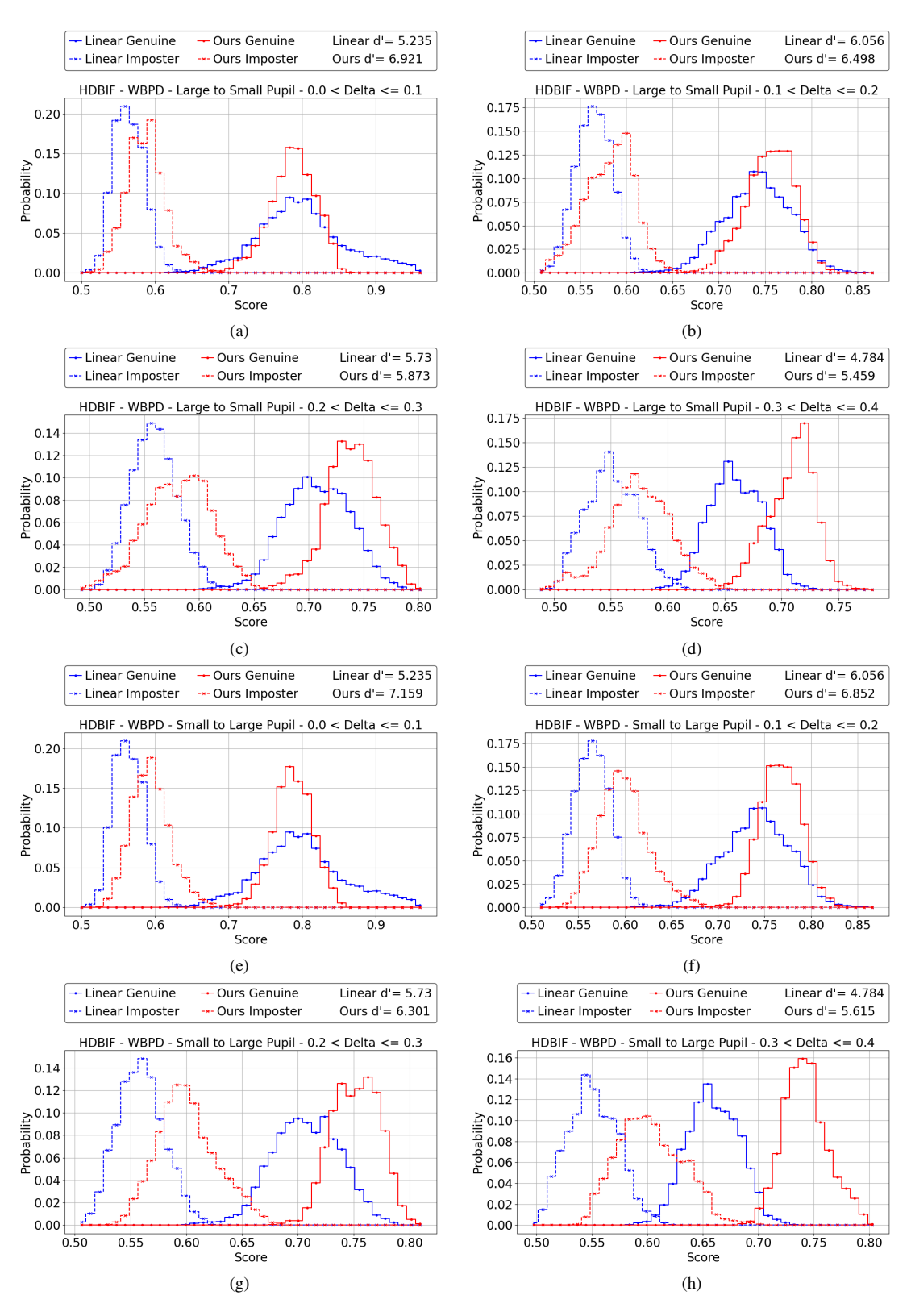


Figure 12. Same as in Fig. 11 except that results for the HDBIF matcher are presented. The scores represent the similarity (1 - [original HDBIF score]).